Instantaneous synthesis of organic-inorganic laccase-cobalt phosphate hybrid nanoflowers: Structural and biocatalytic characterization

Khashayar Vojdanitalab
Tehran University of Medical Sciences
Hossein Jafari-Nodoushan
Tehran University of Medical Sciences
Somayeh Mojtabavi
Tehran University of Medical Sciences
Mahtab Shokri
Tehran University of Medical Sciences
Hoda Jahandar
Islamic Azad University
Mohammad Ali Faramarzi (faramarz@tums.ac.ir)
Tehran University of Medical Sciences

Research Article

Keywords: Bioremoval, Enzyme immobilization, Hybrid nanoflowers, Laccase, Moxifloxacin

Posted Date: February 22nd, 2022

DOI: https://doi.org/10.21203/rs.3.rs-1351173/v1

Abstract

Organic-inorganic hybrid nanoflowers (HNFs) have been synthesized by soft biomineralization procedures and are mainly used in biocatalysis and biosensing. Previously-reported methods for the synthesis of HNFs have so far required a 3-day incubation, bath sonication, or shear stress tension, which possibly introduces damage to the organic component. In this study, a novel method for instant fabrication of laccase@$Co_3(PO_4)_2$•HNFs was developed without using harsh conditions. The prepared HNFs were assembled instantly by the "concentrated method," which resulted in the fast growth of the flower-shaped nanostructures by a higher collision rate of the primary nucleation sites. The obtained results indicated that catalytic efficiency and enzymatic activity of laccase@$Co_3(PO_4)_2$•HNFs were 113% and 110%, respectively, compared to the free enzyme. Also, the stability of the immobilized enzyme was enhanced by 400% in basic pH values. The activity of laccase@$Co_3(PO_4)_2$•HNFs declined to 50% of the initial value after 10 reusability cycles, indicating successful immobilization of the enzyme. Structural studies revealed a 32% increase in the α-helix content after hybridization with cobalt phosphate, which improved the activity and stability of the immobilized laccase. Furthermore, the fabricated HNFs exhibited a considerable ability to remove moxifloxacin as an emerging pollutant. The antibiotic (10 mg/L) was removed by 24% and 75% after 24 h through adsorption and biodegradation mechanisms, respectively. This study introduces a new method for synthesizing HNFs, which could be used for the instant fabrication of efficient biocatalysts, biosensors, and adsorbents to be potentially employed in industrial, biomedical, and environmental applications.

1. Introduction

Over the past two decades, various heterogeneous biocatalysts, immobilized enzymatic active substances, have been developed for environmental and industrial applications[1]. The preparation of new platforms based on organic-inorganic hybrid materials for the immobilization of enzymes is of great interest. Organic-inorganic hybrid nanoflowers (HNFs), the hierarchical three-dimensional nanostructures that were initially discovered in 2012[2]. HNFs, composed of enzyme(s) and inorganic component(s), have a large surface area, facile synthesis procedure, and hierarchical porous structures[3]. After incorporating enzymes into HNFs, their activity, stability, and reusability have notably increased, owing to low mass transfer limitations arising from their high surface-to-volume ratio and cooperative effects between enzymes and metal ions[4]. For instance, the incorporation of lipase into $Zn_3(PO_4)_2$•HNFs resulted in a 147% enhancement of the enzyme activity. Also, the storage stability of the lipase-containing HNFs was three times higher than free lipase[5]. Carbonic anhydrase (CA) was successfully immobilized into $Ca_8H_2(PO_4)_6$•HNFs and exhibited remarkable stability against elevated temperatures (30–80°C). CA@$Ca_8H_2(PO_4)_6$•HNFs retained 100% of their initial CO_2 hydration activity after 5 reusability cycles[6]. Accidental addition of copper sulfate to phosphate buffer saline (PBS) in the presence of bovine serum albumin (BSA) resulted in the synthesis of the flower-shaped BSA@$Cu_3(PO_4)_2$•HNFs[2]. Three approaches have been reported for the preparation of HNFs, including one-step precipitation[2], ultrafast sonication[7],

and shear stress-mediated synthesis[8]. In the one-step precipitation method, a facile and straightforward strategy, fabrication of HNFs requires a long incubation time (1 ~ 3 days). As long synthesis procedure may potentially reduce the stability of the organic constituent, serious attempts have been established to shorten the assembling time. A rapidly ultrafast sonochemical synthesis of laccase@$Cu_3(PO_4)_2$•HNFs was reported using sonication of the reaction mixture within 5 min at room temperature[7]. Introducing shear stress to the organic component and inorganic precursors to synthesize copper-based HNFs was recently reported[8].

Considering the fact that HNFs are at the early stages of development, the formation mechanism of HNFs has not been accurately established. However, it is believed that the formation of primary nucleation sites of metal phosphate(s) and organic molecule(s) (e.g., protein, DNA, etc.) and time-dependent anisotropic growth of these primary nucleation sites[9] are responsible for the formation of the flower-like structures. It seems that by introducing kinetic energy to the precursors, provided by ultrasonication and vortexing, HNFs assembling time was reduced. As efficient biocatalysts, HNFs have been used for the removal of emerging contaminants such as industrial dyes. However, the ability of HNFs for the removal of antibiotics have not been reported previously[4].

Moxifloxacin, as a fourth-generation fluoroquinolone (FQ), is responsible for more than 34.6% of the total FQs consumption in China. It is mostly used for the treatment of pneumonia and skin infections. Recently, due to its usage in severe acute respiratory syndrome coronavirus 2, moxifloxacin consumption has temporarily increased. Therefore, consumption, release, and accumulation of moxifloxacin in the environment may be threatening[10]. Moxifloxacin is also the most toxic FQs against the growth of *Pseudokirchneriella subcaptitata*[11]. Likewise, it exhibited significant negative effects on the growth and reproduction of *Ceriodaphnia dubia* and *Daphnia manga*[12]. Therefore, increased consumption and release of moxifloxacin in the environment may be threatening to the ecosystem and human health. The efficiency of current approaches for the elimination of antibiotics from wastewaters is limited[13]. In this regard, various techniques for the removal of antibiotics have been so far established such as biocatalysis[14], photocatalysis[15], electrocatalysis[16], etc. Laccases, an oxidoreductase enzyme, has been broadly used for environmental and industrial applications[17,18]. Free and immobilized laccases have been incorporated for bioremoval of a wide range of pollutants such as bisphenol A, crystal violet, acid orange-7, levofloxacin, etc.[19–22]

In this study, a novel method for the fast synthesis of HNFs was proposed without incorporating kinetic energy. Laccase@$Co_3(PO_4)_2$•HNFs were instantly synthesized through rapid anisotropic growth of laccase-cobalt phosphate nanocrystals, and a new mechanism was proposed for the synthesis of HNFs. Biocatalytic properties of laccase@$Co_3(PO_4)_2$•HNFs were investigated, and the structure of the hybridized enzyme was also characterized. The synthesized HNFs were then employed to remove moxifloxacin from aqueous media. The degradation products were identified, and their toxicity against four bacteria involved in the degradation of organic compounds was assessed.

2. Experimental

2.1. The enzyme and chemicals

Laccase from *Trametes versicolor* (0.5 U/mg) and 2,2'-azino-bis(3-ethylbenzothiazoline-6-sulfonic acid) (ABTS) were purchased from Sigma-Aldrich (St. Louis, Mo, USA). Cobalt (II) chloride hexahydrate ($CoCl_2.6H_2O$) was obtained from Merck (Darmstadt, Germany). All other applied reagents and chemicals were of analytical grade without further purification. Moxifloxacin was kindly gifted from Soha Pharmaceutical Company (Tehran, Iran).

2.2. Instant synthesis of cobalt-based hybrid nanoflowers with laccase

Regardless of the conventional methods, an instant strategy was applied for the construction of HNFs. The synthesis procedure was accomplished by the addition of 0.1 mL of $CoCl_2$ solution into 0.9 mL of phosphate buffer (pH 7.4) containing 0.1 U mL^{-1} of laccase. Instantly a large number of purple precipitates appeared in the solution. Proper concentration of $CoCl_2$ and molarity of phosphate buffer were subsequently optimized against highest activity recovery (n = 3, *p*-value < 0.05). The precipitates were centrifuged at 6000 *g* and washed three times with phosphate buffer. The purple products were marked as laccase@$Co_3(PO_4)_2$•HNFs.

2.3. Characterization of laccase@$Co_3(PO_4)_2$•HNFs

Scanning electron microscopy (SEM) images (Tescan, MIRA II, Czech Republic) were applied to indicate the flower-shaped morphology of the fabricated HNFs. Energy dispersive X-Ray spectroscopy (EDX, Tescan, MIRA II, Czech Republic) and elemental mapping were incorporated to determine the composition and spatial distribution of elements in the constructed HNFs, respectively. Fourier transform infrared (FTIR) spectroscopy (Shimadzu, Equinox 55, Japan) was utilized for analyzing functional groups of organic and inorganic constituents of HNFs. The samples were dispersed in pressed KBr disks, and the spectra were recorded at 4000–400 cm^{-1}. Brunauer-Emmett-Teller (BET) analysis was performed (Microtrac, BELSORP MINI X, Japan) after degassing the samples under N_2. X-ray diffraction (XRD) analysis was carried out to identify the crystalline phase of the inorganic component using an X-ray diffractometer (Philips, PW1730, Philips, Eindhoven, Netherlands).

2.4. Laccase activity assay

Laccase activity was spectroscopically measured following by oxidation of ABTS as the substrate[23]. Laccase@$Co_3(PO_4)_2$•HNFs and the free enzyme were incubated with ABTS (50 μM, 1 mL) at 40°C in a shaker incubator. After 15 min incubation, the optical density of the supernatants was recorded at 420 nm. One unit of activity was defined as the amount of laccase capable of oxidizing 1 μmol ABTS to the colored product in 1 min. Effect of pH and temperature on the activity of both laccase@$Co_3(PO_4)_2$•HNFs

and the free form of laccase was determined in the temperature range of 25–55°C (interval 10°C) and pH range of 2.5–9.5 (interval 1) (n = 3, *p*-value < 0.05).

2.5. Determination of immobilization yield and efficiency

After preparing laccase@$Co_3(PO_4)_2$•HNFs, the concentration of residual protein in the supernatant was estimated by the bicinchoninic acid (BCA) method (n = 3, *p*-value < 0.05)[24]. Immobilization yield (IY) was calculated using Eq. 1, where Y_0 and Y_1 represent the amount of immobilized enzyme in HNFs before and after the synthesis procedure, respectively (n = 3, *p*-value < 0.05).

$$IY\ (\%) = [(Y_0 - Y_1)/Y_0] \times 100 \quad \text{Eq. 1}$$

The immobilization efficiency (IE) was obtained by Eq. 2, where E_0 and E_t demonstrate the activity of free laccase and laccase@$Co_3(PO_4)_2$•HNFs, respectively.

$$IE\ (\%) = [(E_0 - E_t)/E_0] \times 100 \quad \text{Eq. 2}$$

2.6. Evaluation of the kinetic parameters of the constructed HNFs

In order to assess the influence of immobilization on laccase, kinetic parameters of laccase@$Co_3(PO_4)_2$•HNFs and the free laccase were evaluated. The activity of both the free and immobilized biocatalysts was determined in the presence of ABTS concentrations (20–100 µM). Lineaweaver-Burke plot was incorporated for evaluation of kinetic parameters such as Michaelis constant (K_m) and maximum velocity (V_{max}). Turnover number (K_{cat}) and catalytic efficiency were calculated based on Eqs. 3 and 4[25–27]; where [E] is the concentration of enzyme.

$$K_{cat} = V_{max}/[E] \quad \text{Eq. 3}$$

$$\text{Catalytic efficiency} = K_{cat}/K_m \quad \text{Eq. 4}$$

2.7. Reusability and stability studies

In order to evaluate the reusability of the constructed biocatalyst, repeated measurement of the activity of laccase@$Co_3(PO_4)_2$•HNFs was examined[2]. The fabricated HNFs were incubated in 1 mL phosphate buffer (10 mM, pH 7.4) containing ABTS (0.5 mM) at 40°C for 15 min. After centrifugation of the mixture, OD_{420} of the supernatant was recorded, and the precipitates were washed three times with phosphate buffer (10 mM, pH 7.4). The procedure repeated to the point that the activity of HNFs dropped to below 50% of its initial value (n = 3, *p*-value < 0.05). The stability of the free laccase and HNFs was assessed as a function of recovered activity after 3 h incubation at temperatures ranging 25–55°C (interval 10°C) and a wide pH range of 2.5–9.5 (interval 1). Storage stability of the free laccase and HNFs were obtained by measurement of laccase activity during storage at 4°C (n = 3, *p*-value < 0.05).

2.8. The enzyme structural studies

In order to evaluate the conformational changes of laccase after immobilization, far-UV circular dichroism (CD) and fluorescence spectroscopies were utilized. CD spectra of laccase@$Co_3(PO_4)_2$•HNFs and the free enzyme were recorded by a Jasco 725 spectrophotometer in a 2 mm path-length cell, and the absorbance was recorded at 190–240 nm. The fluorescence property of tryptophan is dependent on the 3rd structure of a protein. In this regard, the tryptophan fluorescence intensity of the free laccase and laccase@$Co_3(PO_4)_2$•HNFs were recorded by a Hitachi 850 spectrofluorometer after excitation at 285 nm[23]. Finally, thermogravimetry analysis (TGA) was using performed using a thermogravimetric analyzer (Perkin Elmer STA 6000, USA) for evaluation of thermal decomposition of both pure cobalt phosphate and laccase@$Co_3(PO_4)_2$•HNFs. The experiment was conducted under an N_2 atmosphere in the temperature range of 25–600°C by a heating rate of 10°C/min.

2.9. Bioremoval experiments

2.9.1. Bioremoval of moxifloxacin

Moxifloxacin was incubated with laccase@$Co_3(PO_4)_2$•HNFs and 1-hydroxybenzotriazole (HBT) as the laccase mediator in phosphate buffer (10 mM, pH 4.5) at 40°C under stirring condition (100 rpm)[28]. After determining the period of incubation, the concentration of moxifloxacin was quantified by high-performance liquid chromatography (HPLC) coupled with UV detector, and the removal percentage was calculated based on Eq. 5 (n = 3, *p*-value < 0.05); as C_0 and C_t represent the concentration of moxifloxacin before and after removal experiments, respectively.

Removal (%)= $(C_0\text{-}C_t/C_0)\times100$ Eq. 5

2.9.2. Sample preparation and quantification of moxifloxacin

After the removal procedure, the pH of the reaction mixture was set to 7.95 (isoelectric point of moxifloxacin) by phosphate buffer (100 mM, 7.95). Then, the mixture was extracted with chloroform under vigorous vortex three times after the addition of ciprofloxacin as the internal standard. The extracted chloroform evaporated to dryness by a rotary evaporator instrument, and the remaining powder was dissolved in 1 mL of the HPLC mobile phase. A Knauer HPLC-UV system (Berlin, Germany) was incorporated for moxifloxacin quantification using a PDA 2800 detector, a Smartline 1000 pump, and ChromGate software (version 3.3.1). The mobile phase consisted of methanol (45%) and 10 mM phosphate buffer (pH 3.0) (55%). Samples were injected by Smartline autosampler 3950 to a Eurospher 100 C18 reversed-phase column (250 × 4.6 mm).

2.9.3. Identification of biotransformation products

Biotransformation products of moxifloxacin were identified by liquid chromatography coupled by mass spectroscopy (LC-MS). The apparatus was an Agilent 1200 series LC system coupled with an Agilent 6520 quadrupole time of flight tandem MS instrument featured by an electrospray ion source (Agilent,

Waldbronn, Germany). A 2.1–100 mm Nucleosil 100 – 3 C18 HD column (Macherey-Nagel, Düren, Germany) was applied with a flow rate of 0.35 mL min^{-1}. Deionized water + 0.1% formic acid (40%) and acetonitrile (60%) were used as mobile phase.

2.9.4. Toxicity of the bioremoval procedure

Based on previous studies, elimination of toxicity is not guaranteed by degradation of antibiotics in catalytic procedures[29]. Accordingly, the toxicity of moxifloxacin degradation products was examined against some bacteria, including *Pseudomonas aeruginosa* ATCC 9027, *Escherichia coli* ATCC 25,922, *Staphylococcus epidermidis* ATCC 49,619, and *Staphylococcus aureus* ATCC 6538, which are responsible for the bioremoval of organic pollutants in the environment. In this regard, the fresh culture of each bacterium was seeded in a nutrient broth and incubated at 37°C overnight. Then, each bacterium was treated with a mixture of degradation products, and the optical density (OD) of each bacterium was evaluated at 600 nm after determining the incubation time periods at 37°C. Growth inhibition of moxifloxacin degradation products, moxifloxacin as the positive control, and sterile water as the negative control were measured by plotting OD_{600} against incubation time (n = 3, *p*-value < 0.05)[22].

2.10. Analysis of the experiments

The experiments were conducted in triplicate, and results were reported as mean ± standard deviation. Statistical significance among the mean value of experimental results was calculated by two-way ANOVA (± standard deviation) and p-value < 0.05 regarded as significant.

3. Results And Discussion

3.1. Instant synthesis of laccase@$Co_3(PO_4)_2$•HNFs

HNFs have been routinely constructed with the addition of metal ions to enzyme-containing PBS followed by a 3-day incubation at room temperature, vigorous vortexing, or bath sonication, which introduces significant stress to the organic constituent[2,7,9,30]. In the present study, the concentration of $CoCl_2$ and molarity of phosphate buffer (pH 7.4) were optimized to instantly fabricate HNFs and avoid incorporating stress-inducing conditions in the synthesis procedure. After the addition of $CoCl_2$ to laccase-containing phosphate buffer, the purple precipitates were immediately formed. The precipitate was washed with deionized water three times and designated as laccase@$Co_3(PO_4)_2$•HNFs. As shown in Fig. 1a, the recovered activity increased gradually at the higher molarity of phosphate buffer. However, the highest activity recovery was obtained with HNFs prepared with 0.16 M phosphate buffer and 30 mM $CoCl_2$. Effects of bath sonication (60 kHz, 13.8 W) or incubation at 25°C (24–72 h) on the activity recovery were also evaluated. The results (Fig. 1b) demonstrated that further incubation reduced the recovered activity. Also, sonication of the reaction mixture (up to 20 min, 5 min intervals) did not increase the recovered activity. The mentioned synthesis method is referred to as the “concentrated method” in the present study for comparison with the up to now reported and traditional procedures. The present explanation of the

formation mechanism of HNFs is based on the nucleation of primary metal phosphate-protein nanocrystals and subsequent anisotropic growth of the hybrid nanoaggregates. Due to the high surface energy of the primary protein-inorganic nanocrystals, they tend to attach and form the nano-sheet structures, which finally form the ultimate structure of HNFs[3]. The growth of nucleation sites of HNFs could be facilitated by increasing the collision rate of the primary crystals[31]. It seems that introduction of certain amounts of kinetic energy, provided by long-term incubation (24–72 h at 25°C), bath sonication, microwave heating, and shear stress, to the synthesis mixture (organic component, metal, and phosphate ions) could induce the formation of HNFs. The number of primary nucleation sites increased by incorporating a high concentration of Cobalt (II) and phosphate ions in the reaction mixture. Hence, based on Eq. 6, higher numbers of nanocrystals possibly collide together more frequently, and HNFs were prepared very fast[31]. In Eq. 6, z is collision frequency, D is the particle diameter, $\bar{\upsilon}$ represents the mean velocity of dispersed particles, N is the total number of particles, and V is the total volume of the reaction mixture.

$$z = (\sqrt{2}\pi D^2 \bar{\upsilon} N) \times V^{-1} \quad \text{Eq. 6}$$

Hybrid nanoflowers have been synthesized in a short period of time through vigorous vortexing[8] and also bath sonication[7] of the precursors, which increased the mean velocity of the dispersed particles ($\bar{\upsilon}$). Based on Eq. 6, after the increase in the mean velocity of dispersed organic-inorganic particles by vortexing or bath sonication, the collision frequency increases, which results in fast anisotropic growth of the HNFs.

3.2. Characterization of laccase@$Co_3(PO_4)_2$•HNFs

The flower-shaped morphology of the fabricated HNFs (Fig. 2a) was confirmed by SEM image. The size of laccase@$Co_3(PO_4)_2$•HNFs ranged 0.5–3 μm and was assembled by interconnected nano-sheets resulting high surface-to-volume ratio (Fig. 2b). Cobalt phosphate nanoflowers (NFs) were also prepared through the same synthetic route without the incorporation of laccase in the reaction mixture. As shown in Fig. S1 and S2, the cobalt phosphate•NFs also exhibited flower-like morphology. Some of the previous studies reported that the flower-shaped morphology of HNFs is due to the presence of inorganic constituent(s)[32,33]. Also, it was reported that the 3D structure of the incorporated organic component could alter the morphology of HNFs[34]. However, inorganic copper phosphate was prepared by the same synthesis procedure, which exhibited the same flower-shaped morphology as protein@$Cu_3(PO_4)_2$•HNFs[35–38]. All in all, it could be concluded that some metal phosphates have flower-like morphology[39] that could be modified after hybridization with proteins. EDX analysis of laccase@$Co_3(PO_4)_2$•HNFs and cobalt phosphate nanoflowers are exhibited in Fig. 2d and Fig. S4, respectively. The weight percentage of elements in both constructed HNFs and cobalt phosphate is summarized in Table S1. The presence of nitrogen atoms in the prepared HNFs confirms the immobilization of laccase into the support. Elemental map analysis (Fig. 2c) also provides information on the homogenous distribution of Co, P, N, and O atoms in the constructed HNFs. In order to identify the

inorganic part of laccase@$Co_3(PO_4)_2$•HNF, the XRD analysis was performed. The obtained peaks of laccase@$Co_3(PO_4)_2$•HNF were in good agreement with the standard cobalt phosphate pattern (JCPDS 00-027-1120) (Fig. 3). Mean pore diameter, total pore volume, and specific surface area of the fabricated HNFs and $Co_3(PO_4)_2$•NFs are summarized in Table S2, and corresponding BET plots are shown in Fig. S5. The high specific surface area (17.42 m^2/g) is in agreement with the nano-sized width of petals in the SEM image of laccase@$Co_3(PO_4)_2$. As shown, the specific surface area of $Co_3(PO_4)_2$•NFs and the synthesized HNFs was almost identical. The presence of type IV isotherm in the BET plots is due to the mesoporous structure of the synthesized materials. As a rule of thumb, the higher surface area of the immobilized enzyme increases the accessibility of substrate to the enzyme and enhances the biocatalytic efficiency[40]. The same results were reported for laccase@$Cu_3(PO_4)_2$•HNFs (10.2 m^2/g) and GOx@$Cu_3(PO_4)_2$•HNFs (17.9 m^2/g)[41,42]. FTIR spectra of laccase, $Co_3(PO_4)_2$, and laccase@$Co_3(PO_4)_2$•HNFs are represented in Fig. 4a. As shown, characteristic vibrational frequencies in the region 725–1300 cm^{-1} are due to the presence of phosphate groups [43]. Peaks at 2980–3600 cm^{-1} attributed to the presence of CH_2 and CH_3 groups in laccase@$Co_3(PO_4)_2$•HNFs[43]. The broad band in 3200–3500 cm^{-1} corresponds to O-H starching band[44]. A peak at 1640 cm^{-1} is attributed to the amide (II) band of laccase; however, the peak is overlapped with entrapped water peak of laccase@$Co_3(PO_4)_2$•HNFs at 1640 cm^{-1} [45,46].

3.3. Structural studies

CD spectra were applied to elucidate the effect of immobilization on the secondary structure of laccase (Fig. S6). As summarized in Table 1, the conformation of the free native laccase was mainly composed of β-sheets (46.4%), β-turns (12.3%), and random coils (41.4%). Nevertheless, the amount of α-helix in the secondary structure of laccase increased remarkably (32%) after the immobilization of laccase in cobalt-based HNFs. The content of β-turns decreased slightly; however, β-sheets content (10.3%) of the laccase was significantly reduced. Laccase from *T. versicolor* is mainly composed of β-sheets, β-turns, and other structures, as reported previously[47,48]. Higher α-helix contents result in a more rigid protein structure, arising from the formation of a higher number of hydrogen bonds. Thus, by decreasing β-sheets and increasing α-helix contents, the laccase secondary structure became more rigid[49]. At first glance, it is not far-fetched that enzyme activity diminishes completely after such alteration in the protein structure. However, the immobilization of enzymes may significantly change the protein structure without loss of activity. For instance, by the preparation of cross-linked enzyme aggregates, the 3D structure of the enzyme is remarkably changed. Cross-linked laccase aggregated have been used for immobilization of the enzyme; meanwhile, the biocatalytic activity of the enzyme was preserved[50–52]. In order to verify the effect of any change in laccase tertiary structure, fluorescence spectroscopy was employed. The surrounding microenvironment highly influences the fluorescence properties of tryptophan; consequently, any change in the tryptophan microenvironment represents protein folding. As shown in Fig. S7, the fluorescence intensity of laccase@$Co_3(PO_4)_2$•HNFs was lower than the free enzyme, which indicates the considerable change in the 3rd protein structure[53]. The results indicate that immobilization of laccase

into cobalt phosphate HNFs increased the content of α-helix, which ultimately changes the 3rd structure of the protein. As shown in Fig. S8, the weight loss of laccase@$Co_3(PO_4)_2$•HNFs was higher than the pure inorganic nanoflowers, which indicates that 5% of the weight of HNFs is composed of laccase. The total weight loss of laccase@$Co_3(PO_4)_2$•HNFs upon decomposition was 32.02%. The initial weight loss of samples (6% at 100–160°C) was due to the evaporation of crystal water entrapped in cobalt phosphate. At the second stage, the weight loss is attributed to the decomposition of immobilized laccase, which was 22%.

Table 1
Secondary structures content of the free laccase and laccase@$Co_3(PO_4)_2$•HNFs.

Type of catalyst	α-Helix (%)	β-Sheet (%)	β-Turns (%)	Random coils (%)
The free laccase	5	44.4	11.3	39.4
Laccase@$Co_3(PO_4)_2$•HNFs	32	10.3	6.5	51.2
* $p < 0.05$ vs. the free laccase				

3.4. Enzyme activity of laccase@$Co_3(PO_4)_2$•HNFs against temperatures and pH values

In order to determine the optimum conditions for the activity of laccase@$Co_3(PO_4)_2$•HNFs, the enzyme activity was measured in a broad range of pH and temperature. As shown in Fig. 5a and 5b, the activity of the laccase@$Co_3(PO_4)_2$•HNFs in basic pH values was remarkably higher than the free enzyme. However, maximum activity of both laccase@$Co_3(PO_4)_2$•HNFs and the free enzyme was obtained at a pH range of 4.5–5.5 and 45°C. This phenomenon could be due to the higher surface area of laccase@$Co_3(PO_4)_2$•HNFs that enhance the enzyme activity[54]. It is believed that high temperatures and extreme acidic or basic pH reduce the activity and stability of the enzymes by induction of conformational changes[55]. However, it was shown that hybridization of nitrile hydratase (NHase) with cobalt phosphate complexes increased the stability of NHase against temperature[56]. Similarly, the activity of laccase was increased by 165% after incorporation into laccase@$Cu_3(PO_4)_2$•HNFs[55]. Stable coordination of laccase with cobalt phosphate probably results in higher operational stability of the enzyme.

3.5. Estimation of immobilization yield, efficacy, and kinetic parameters

Due to the improved enzymatic activity of the synthesized HNFs in basic pH values, kinetic properties of the immobilized and free laccase were evaluated in pH 4.5 and 7.4. Immobilization yield, efficiency, and kinetic properties of instantly-prepared laccase@$Co_3(PO_4)_2$•HNFs and the free enzyme are summarized in Table 2. Immobilization efficiency, V_{max} and K_m of the biocatalysts were different in basic and acidic conditions. The V_{max} value of the laccase@$Co_3(PO_4)_2$•HNFs at pH 7.4 was 40% higher than pH 4.5;

however, the maximum velocity of the free enzyme declined 21.2% at pH 7.4. Likewise, the efficiency of the immobilization procedure was increased by 25% in pH 7.4. The results indicated that K_{cat} of laccase@$Co_3(PO_4)_2$•HNFs was higher than the free enzyme at pH 7.4; while, the free enzyme exhibited superior K_{cat} over laccase@$Co_3(PO_4)_2$•HNFs at pH 4.5. These results are in alignment with the effect of pH on the activity of both free and immobilized laccase. The Michaelis constant (K_m) indicates the affinity of the enzyme toward the substrate, and a low K_m value indicates the high affinity of the enzyme toward the substrate in both pH values. The improved accessibility of laccase@$Co_3(PO_4)_2$•HNFs to the substrate (compared to the free enzyme) could be attributed to the high surface area of the flower-shaped structures that reduces the mass transfer limitations[54]. Normally, K_m, V_{max}, and the optimum conditions for reaching the highest catalytic efficiency enzymes may alter after immobilization[57]. Maximum activity of fungal laccases has been reported to be obtainable at a pH range of 3 – 5[58]. One of their main limitations is an insufficient activity in neutral and alkaline conditions despite the high redox potential of fungal laccases (490–790 mV). In this regard, pH-tolerant laccases are desirable for industrial and environmental purposes[59]. Hybridization of laccase with cobalt phosphate nanocrystals enhanced the tolerance of laccase from *T. versicolor* toward alkaline conditions, which could improve their desirability for industrial and environmental applications[60].

Table 2
Kinetic parameters of the free laccase and laccase@$Co_3(PO_4)_2$•HNFs.

Parameter	**The free laccase**		**Laccase@$Co_3(PO_4)_2$•HNFs**	
	pH		**pH**	
	4.5	**7.4**	**4.5**	**7.4**
V_{max} (µmol/min)	8.4 ± 0.4	6.2 ± 0.2	4.7 ± 0.2	6.6 ± 0.3
K_m (µM)	147.9 ± 8.5	118.5 ± 5.3	85.4 ± 4.3	110.7 ± 4.6
$K_{cat} \times 10^{-2}$ (S^{-1})	6.5 ± 0.2	4.8 ± 0.2	3.6 ± 0.1	5.1 ± 0.1
Catalytic efficiency $\times 10^{-4}$ (K_{cat}/ K_m)	4.4 ± 0.3	4.0 ± 0.2	4.2 ± 0.3	4.6 ± 0.4
Immobilization yield (%)	-	-	65.3 ± 7.6	65.3 ± 7.6
Immobilization efficacy (%)	-	-	86 ± 5.3	110 ± 4.9

3.6. Reusability and stability of laccase@$Co_3(PO_4)_2$•HNFs

Reusability is an important feature of biocatalysts that reduces their utilization cost, especially on the industrial scale[61]. However, in the present study, measurement of the reusability for laccase@$Co_3(PO_4)_2$•HNFs provided evidence on the successful immobilization of laccase into the matrix of cobalt phosphate. In order to evaluate the reusability of laccase@$Co_3(PO_4)_2$•HNFs, the enzyme activity

was consecutively measured by ABTS as the substrate. As shown in Fig. 4b, after 4 consecutive reuse cycles, the activity of the laccase@$Co_3(PO_4)_2$•HNFs did not significantly change. However, the residual activity declined to 50% of its initial value after 10 cycle reuses. The results indicate that laccase@$Co_3(PO_4)_2$•HNFs exhibited remarkable reusability, and the enzyme was successfully immobilized in the matrix of cobalt phosphate. Laccase-based HNFs were exhibited promising reusability; for instance, laccase and lysin-copper HNFs retained 60% of initial activity after 6 cycles of reusability[62]. In another study, laccase-copper HNFs retained 50% of the initial activity after 10 reusability runs; however, the glutaraldehyde-treated HNFs retained almost 100% of their initial activity at the same conditions[63]. As shown in Fig. 5c and 5d, the stability of laccase@$Co_3(PO_4)_2$•HNFs against elevated temperatures and basic pH values was higher than the free laccase. Laccase@$Co_3(PO_4)_2$•HNFs retained 50% of their activity after incubation at pH 9.5 for 3 h, where the free laccase almost lost all of its activity. It should be noted that the stability of laccase@$Co_3(PO_4)_2$•HNFs was lower than the free enzyme in acidic pH values due to the solubility of cobalt phosphate in acidic pH[64]. No data is available for comparison. As mentioned in 3.3, the α-helix content of laccase was increased after hybridization with cobalt phosphate. Copper ions of laccase, which are involved in the catalytic activity of the enzyme, are present in β-sheets, which are mainly composed of conserved polar amino acids[65]. The stability and activity of laccase have been reported to be increased when the content of α-helix increased and β-sheets decreased[22,49,66]. A more rigid protein structure aligned with increasing in α-helix content could explain the higher stability of laccase HNFs than the free enzyme[22]. However, the stability of enzymes immobilized on cobalt-based supports was enhanced[67]. The thermal stability of laccase-based HNFs was previously reported[54,55]. Immobilization of laccase into laccase@$Co_3(PO_4)_2$•HNFs increased the storage stability of the enzyme. As shown in Fig. 4c, after 40 days of storage at 25°C, the prepared HNFs retained 20% of the initial activity, while the free enzyme lost 58% of the initial activity.

3.7. Bioremoval of moxifloxacin

As shown in Fig. 4d, laccase@$Co_3(PO_4)_2$•HNFs were able to degrade moxifloxacin significantly. However, due to the propensity of FQ antibiotics to adsorb onto inorganic surfaces, the possible adsorption of moxifloxacin on the synthesized HNFs was evaluated[13,68–70]. In order to specifically determine the adsorption of moxifloxacin on the constructed HNFs, the immobilized laccase was deactivated by sequential freeze and thawing cycles. Adsorption of moxifloxacin on the surface of HNFs reached a plateau after 18 h of incubation. The maximum adsorptive capacity of inactivated laccase@$Co_3(PO_4)_2$•HNFs for moxifloxacin was found to be 0.8 mg/g. The laccase@$Co_3(PO_4)_2$•HNFs completely removed moxifloxacin from the reaction mixture. Due to the high surface of HNFs, the adsorption of organic and inorganic components is not farfetched. There are some reports on the ability of HNFs for adsorption of cadmium and doxorubicin[36,71].

3.8. Identification of degradation products

After the bioremoval procedure, the mixture of moxifloxacin biotransformed products was subjected to LC-MS analysis. The main by-products, their retention times, and corresponding mass to charge ration (m/z) are presented in Fig. S9. Based on the LC-MS results, five plausible pathways for the degradation of moxifloxacin are proposed (Fig. 6). Interestingly, the biocatalyst replaced the fluorine atoms from moxifloxacin, which is responsible for the low biodegradability of FQs, with hydroxyl groups (compound III; m/z + 1 = 262, R_t = 6 min)[72]. As shown, ring-opening of piperazine moiety and further demethylation reactions were responsible for appearing compound VI (m/z = 307, trace) and compound II (m/z + 1 = 280, R_t = 3.9 min), respectively (pathway I). In pathway II, moxifloxacin underwent defluorination and cleavage of the piperazine moiety (compound VII; m/z = 388, trace) and further transformed to compound V (m/z = 358, R_t = 9 min) after dihydroxylation and demethylation[73]. In the 3rd pathway, by oxidation and opening of piperazine ring, compound VIII (m/z = 418, trace) was formed, which finally converted to compound IV (m/z = 294, R_t = 8.7 min) after subsequent oxidation steps. In the next pathway, compound VIII (m/z = 418, trace) was formed, and by complete cleavage of piperazine group, compound I was transformed to compound IX (m/z = 307, trace) that was transformed to compound VIII (m/z = 294, R_t = 8.7 min) after demethylation and cracking of cyclopropane ring (pathway IV). In the final proposed mechanism, moxifloxacin fluor atom was substituted with OH (compound X, m/z = 400, trace) and further, by loss of piperazine group and demethylation, converted to compound III (m/z + 1 = 262, R_t = 6 min) (pathway V).

3.9. Toxicity of the biodegradation products

Diminishing toxicity of pollutants is not always guaranteed by degradation procedures; even there are reports on an increase in toxicity of pollutants after degradation[74,75]. In order to examine the efficiency of the synthesized HNFs, the toxicity of moxifloxacin and its metabolites against four bacterial strains was evaluated. As shown in Table S3, the toxicity of the degradation products was effectively decreased after treatment with laccase@$Co_3(PO_4)_2$•HNFs. Treatment of moxifloxacin with the constructed HNFs reduced the GI% for *P. aeruginosa* by 67%. GI% reduction for *S. aureus, S. epidermidis*, and *E. coli* was 24.6%, 48.7%, and 12%, respectively. Some of the FQs degradation products exhibited antimicrobial activity. Due to the enhancement of DNA gyrase activity by fluorine, the defluorination of moxifloxacin significantly reduced its biological activity. Also, most of the identified degradation products possess lower hydrophobicity, which may limit their diffusion through the cell membrane[73,76,77].

4. Conclusion

This study reported a facile method for the instant synthesis of HNFs. Contrary to previously-reported synthesis procedures, high concentrations of phosphate and cobalt ions were incorporated for the synthesis of HNFs. The formation of primary nucleation sites (protein-inorganic nanocrystals) and their anisotropic growth are the main steps involved in the synthesis of HNFs by the “concentrated method.” Rapid fabrication of HNFs was achieved by increasing the number of primary nanocrystals, which improved their collision rate and accelerated the growth of HNFs. Catalytic efficiency, kinetic parameters, and stability of laccase were enhanced after the immobilization of enzymes into HNFs. Based on CD and

fluorimetry spectra, higher α-helix content of laccase@$Co_3(PO_4)_2$•HNFs than the free enzyme is responsible for the enhanced stability of the constructed HNFs. The ability of laccase@$Co_3(PO_4)_2$•HNFs to remove moxifloxacin was also assessed. The antibiotic was removed through adsorption and biodegradation mechanisms. The toxicity of degradation products against two G^+ and two G bacteria was remarkably lower than parent fluoroquinolone.

Declarations

Data availability

All data generated or analysed during this study are included in this published article (and its Supplementary Information files).

Author contributions

Khashayar Vojdanitalab: Conceptualization, Methodology, Investigation, and Writing - Original Draft. Hossein Jafari: Data curation, Writing- Original draft preparation, Visualization, and Software. Somayeh Mojtabavi*:* Formal analysis, Writing - Review & Editing, and Conceptualization. Mahtab Shokri: Visualization, Investigation, and Methodology. Hoda Jahandar: Software, Validation, and Investigation. Mohammad Ali Faramarzi: Supervision, Conceptualization, Methodology, Resources, Data Curation, Writing - Review & Editing, Project administration, and Funding acquisition.

Acknowledgment

This work was financially supported by grant number 1400-2-104-54845 from Biotechnology Research Center*,* Tehran University of Medical Sciences, Tehran, Iran, to M.A.F.

Competing interest statement

The author(s) declare no competing interests.

References

1. Kovalenko, G. & Perminova, L. Heterogeneous biocatalysts for the final stages of deep processing of renewable resources into valuable products. Molecular Biotechnology (2020) doi:10.5772/INTECHOPEN.89411.
2. Ge, J., Lei, J. & Zare, R. N. Protein-inorganic hybrid nanoflowers. Nature Nanotechnology **7**, 428–432 (2012).
3. Liu, Y., Ji, X. & He, Z. Organic–inorganic nanoflowers: From design strategy to biomedical applications. Nanoscale **11**, 17179–17194 (2019).
4. Bilal, M., Asgher, M., Shah, S. Z. H. & Iqbal, H. M. N. Engineering enzyme-coupled hybrid nanoflowers: The quest for optimum performance to meet biocatalytic challenges and opportunities. International

Journal of Biological Macromolecules **135**, 677–690 (2019).

5. Zhang, B. *et al.* Preparation of lipase/$Zn_3(PO_4)_2$ hybrid nanoflower and its catalytic performance as an immobilized enzyme. Chemical Engineering Journal **291**, 287–297 (2016).
6. Duan, L., Li, H. & Zhang, Y. Synthesis of hybrid nanoflower-based carbonic anhydrase for enhanced biocatalytic activity and stability. ACS Omega **3**, 18234–18241 (2018).
7. An, S. S., Park, H. G., Kim, M. il, Batule, B. & Park, K. S. Ultrafast sonochemical synthesis of protein-inorganic nanoflowers. International Journal of Nanomedicine **10**, 137142 (2015).
8. Carey, A. B., Cai, W., Gibson, C. T., Raston, C. L. & Luo, X. Shear stress-mediated growth of cupric phosphate Nnanostructures. Crystal Growth & Design **21**, 4579–4586 (2021).
9. Lee, S. W., Cheon, S. A., Kim, M. il & Park, T. J. Organic–inorganic hybrid nanoflowers: types, characteristics, and future prospects. Journal of Nanobiotechnology **13**, 54 (2015).
10. Wan, L. *et al.* Effects of moxifloxacin and gatifloxacin stress on growth, photosynthesis, antioxidant responses, and microcystin release in *Microcystis aeruginosa*. Journal of Hazardous Materials **409**, 124518 (2021).
11. van Doorslaer, X. *et al.* Heterogeneous photocatalysis of moxifloxacin in water: Chemical transformation and ecotoxicity. Chemosphere **119**, S75–S80 (2015).
12. Kergaravat, S. v, Hernández, S. R. & Gagneten, A. M. Second-, third- and fourth-generation quinolones: Ecotoxicity effects on *Daphnia* and *Ceriodaphnia* species. *Chemosphere* **262**, 127823 (2021).
13. Cuprys, A. *et al.* Fluoroquinolones metal complexation and its environmental impacts. Coordination Chemistry Reviews **376**, 46–61 (2018).
14. Yang, L.-H. *et al.* Biodegradation of sulfonamide antibiotics through the heterologous expression of laccases from bacteria and investigation of their potential degradation pathways. Journal of Hazardous Materials **416**, 125815 (2021).
15. van Doorslaer, X., Dewulf, J., de Maerschalk, J., van Langenhove, H. & Demeestere, K. Heterogeneous photocatalysis of moxifloxacin in hospital effluent: Effect of selected matrix constituents. Chemical Engineering Journal **261**, 9–16 (2015).
16. Ma, J.-F. *et al.* Rational design of biogenic Pd^xAu^y nanoparticles with enhanced catalytic performance for electrocatalysis and azo dyes degradation. Environmental Research **204**, 112086 (2022).
17. Bilal, M. *et al.* Harnessing the biocatalytic attributes and applied perspectives of nanoengineered laccases—A review. International Journal of Biological Macromolecules **166**, 352–373 (2021).
18. Daronch, N. A., Kelbert, M., Pereira, C. S., de Araújo, P. H. H. & de Oliveira, D. Elucidating the choice for a precise matrix for laccase immobilization: A review. Chemical Engineering Journal **397**, 125506 (2020).
19. Ramírez-Montoya, L. A., Hernández-Montoya, V., Montes-Morán, M. A. & Cervantes, F. J. Correlation between mesopore volume of carbon supports and the immobilization of laccase from *Trametes*

versicolor for the decolorization of Acid Orange 7. Journal of Environmental Management **162**, 206–214 (2015).

20. Zhang, J., Ding, S., Ge, Y. & Li, Z. Enhanced removal of crystal violet in water using a facile-fabricated and environmental-friendly laccase immobilized composite membrane. Process Biochemistry **98**, 122–130 (2020).
21. Ademakinwa, A. N. A heat-resistant intracellular laccase immobilized via cross-linked enzyme aggregate preparation: Characterization, application in bisphenol A removal and phytotoxicity evaluation. Journal of Hazardous Materials **419**, 126480 (2021).
22. Najafabadipour, N., Mojtabavi, S., Jafari-Nodoushan, H., Samadi, N. & Faramarzi, M. A. High efficiency of osmotically stable laccase for biotransformation and micro-detoxification of levofloxacin in the urea-containing solution: Catalytic performance and mechanism. Colloids and Surfaces B: Biointerfaces **207**, 112022 (2021).
23. Mojtabavi, S., Jafari, M., Samadi, N., Mehrnejad, F. & Ali Faramarzi, M. Insights into the Molecular-Level details of betaine interactions with Laccase under various thermal conditions. Journal of Molecular Liquids 116832 (2021).
24. Taghizadeh, T. *et al.* Biodegradation of bisphenol A by the immobilized laccase on some synthesized and modified forms of zeolite Y. Journal of Hazardous Materials **386**, 121950 (2020).
25. Cui, C. *et al.* Fabrication of an in-situ co-immobilized enzyme in mesoporous silica for synthesizing GSH with ATP regeneration. Molecular Catalysis **486**, 110870 (2020).
26. Suman, S. K. *et al.* Potential of *Trametes maxima* IIPLC-32 derived laccase for the detoxification of phenolic inhibitors in lignocellulosic biomass prehydrolysate. International Biodeterioration & Biodegradation **133**, 1–8 (2018).
27. Li, X., Zhao, J., Fu, J., Pan, Y. & Li, D. Sequence analysis and biochemical properties of an acidophilic and hyperthermophilic amylopullulanase from *Thermofilum pendens*. International Journal of Biological Macromolecules **114**, 235–243 (2018).
28. Palvannan, T. *et al.* Efficient transformation of phenyl urea herbicide chloroxuron by laccase immobilized on zein polyurethane nanofiber. Journal of Molecular Catalysis B: Enzymatic **99**, 156–162 (2014).
29. Mani, P. *et al.* Degradation of azo dye (Acid Orange 7) in a microbial fuel cell: Comparison between anodic microbial-mediated reduction and cathodic laccase-mediated oxidation. Frontiers in Energy Research **7**, 101 (2019).
30. Luo, X. *et al.* Vortex fluidic-mediated fabrication of fast gelated silica hydrogels with embedded laccase nanoflowers for real-time biosensing under flow. ACS Applied Materials & Interfaces **12**, 51999–52007 (2020).
31. Ribeiro, C., Lee, E. J. H., Longo, E. & Leite, E. R. A kinetic model to describe nanocrystal growth by the oriented attachment mechanism. ChemPhysChem **6**, 690–696 (2005).
32. Hao, M., Fan, G., Zhang, Y., Xin, Y. & Zhang, L. Preparation and characterization of copper-*Brevibacterium* cholesterol oxidase hybrid nanoflowers. International Journal of Biological

Macromolecules **126**, 539–548 (2019).

33. Nadar, S. S., Gawas, S. D. & Rathod, V. K. Self-assembled organic-inorganic hybrid glucoamylase nanoflowers with enhanced activity and stability. International Journal of Biological Macromolecules **92**, 660–669 (2016).
34. Kaur, H., Bari, N. K., Garg, A. & Sinha, S. Protein morphology drives the structure and catalytic activity of bio-inorganic hybrids. International Journal of Biological Macromolecules **176**, 106–116 (2021).
35. Song, G. *et al.* Direct and ultrafast preparation of $Cu_3(PO_4)_2$ nanoflower by ultrasonic spray method without protein assistant and its applications: Large-scale simulation and catalytic reduction. Journal of Molecular Liquids **328**, 115348 (2021).
36. Gao, L., He, Q., Xing, J. & Ge, Z. Removal of doxorubicin by magnetic copper phosphate nanoflowers for individual urine source separation. Chemosphere **238**, 124690 (2020).
37. Luo, Y.-K., Song, F., Wang, X.-L. & Wang, Y.-Z. Pure copper phosphate nanostructures with controlled growth: A versatile support for enzyme immobilization. CrystEngComm **19**, 2996–3002 (2017).
38. He, G., Hu, W. & Li, C. M. Spontaneous interfacial reaction between metallic copper and PBS to form cupric phosphate nanoflower and its enzyme hybrid with enhanced activity. Colloids and Surfaces B: Biointerfaces **135**, 613–618 (2015).
39. Vinothkumar, V. *et al.* Preparation of three dimensional flower-like cobalt phosphate as dual functional electrocatalyst for flavonoids sensing and supercapacitor applications. Ceramics International **47**, 29688–29706 (2021).
40. Datta, S., Christena, L. R. & Rajaram, Y. R. S. Enzyme immobilization: an overview on techniques and support materials. 3 Biotech **3**, 1–9 (2013).
41. Chung, M. *et al.* Ultrarapid sonochemical synthesis of enzyme-incorporated copper nanoflowers and their application to mediatorless glucose biofuel cell. Applied Surface Science **429**, 203–209 (2018).
42. Lee, I. *et al.* Glucose oxidase-copper hybrid nanoflowers embedded with magnetic nanoparticles as an effective antibacterial agent. International Journal of Biological Macromolecules **155**, 1520–1531 (2020).
43. Altinkaynak, C. Hemoglobin–metal^{2+} phosphate nanoflowers with enhanced peroxidase-like activities and their performance in the visual detection of hydrogen peroxide. New J. Chem. **45**, 1573–1583 (2021).
44. Tomanin, P. P. *et al.* Cobalt phosphate nanostructures for non-enzymatic glucose sensing at physiological pH. ACS Applied Materials & Interfaces **10**, 42786–42795 (2018).
45. Zhang, Y. *et al.* An electrochemical paracetamol sensor based on layer-by-layer covalent attachment of MWCNTs and a G4.0 PAMAM modified GCE. Anal. Methods **8**, 2218–2225 (2016).
46. Lasch, P., Diem, M. & Naumann, D. FT-IR microspectroscopic imaging of prostate tissue sections. in *Biomedical Vibrational Spectroscopy and Biohazard Detection Technologies* (eds. Gryczynski, Z. et al.) vol. 5321 1–9 (SPIE, 2004).

47. Galai, S., de los Ríos, A., Hernández-Fernández, F. J., Haj Kacem, S. & Tomas-Alonso, F. Over-activity and stability of laccase using ionic liquids: screening and application in dye decolorization. RSC Adv. **5**, 16173–16189 (2015).
48. Marschelke, C. *et al.* Hairy particles with immobilized enzymes: Impact of particle topology on the catalytic activity. ACS Applied Materials & Interfaces **11**, 1645–1654 (2019).
49. Kumar, A., Ahlawat, S., Mohan, H. & Sharma, K. K. Stabilization–destabilization and redox properties of laccases from medicinal mushroom *Ganoderma lucidum* and human pathogen *Yersinia enterocolitica*. International Journal of Biological Macromolecules **167**, 369–381 (2021).
50. Cabana, H., Jones, J. P. & Agathos, S. N. Preparation and characterization of cross-linked laccase aggregates and their application to the elimination of endocrine disrupting chemicals. Journal of Biotechnology **132**, 23–31 (2007).
51. Primožič, M., Kravanja, G., Knez, Ž., Crnjac, A. & Leitgeb, M. Immobilized laccase in the form of (magnetic) cross-linked enzyme aggregates for sustainable diclofenac (bio)degradation. Journal of Cleaner Production **275**, 124121 (2020).
52. Kumar, V. V., Sivanesan, S. & Cabana, H. Magnetic cross-linked laccase aggregates — Bioremediation tool for decolorization of distinct classes of recalcitrant dyes. Science of The Total Environment **487**, 830–839 (2014).
53. Hellmann, N. & Schneider, D. Hands On: Using tryptophan fluorescence spectroscopy to study protein structure. in *Protein Supersecondary Structures: Methods and Protocols* (ed. Kister, A. E.) 379–401 (Springer New York, 2019). doi:10.1007/978-1-4939-9161-7_20.
54. Li, H. *et al.* Graphene oxide-enzyme hybrid nanoflowers for efficient water soluble dye removal. Journal of Hazardous Materials **338**, 93–101 (2017).
55. Zhu, P. *et al.* Preparation and application of a chemically modified laccase and copper phosphate hybrid flower-like biocatalyst. Biochemical Engineering Journal **144**, 235–243 (2019).
56. Song, Y. *et al.* Preparation of a flowerlike nanobiocatalyst system via biomimetic mineralization of cobalt phosphate with enzyme. Industrial & Engineering Chemistry Research **56**, 14923–14930 (2017).
57. Guzik, U., Hupert-Kocurek, K. & Wojcieszynska, D. Immobilization as a strategy for improving enzyme properties-application to oxidoreductases. Molecules **19**, 8995–9018 (2014).
58. Yin, Q. *et al.* The first fungal laccase with an alkaline pH optimum obtained by directed evolution and its application in indigo dye decolorization. AMB Express **9**, 1–13 (2019).
59. Torres-Salas, P. *et al.* Widening the pH activity profile of a fungal laccase by directed evolution. ChemBioChem **14**, 934–937 (2013).
60. Novoa, C. *et al.* KnowVolution of a fungal laccase toward alkaline pH. ChemBioChem **20**, 1458–1466 (2019).
61. Torres, J. A. *et al.* Development of a reusable and sustainable biocatalyst by immobilization of soybean peroxidase onto magnetic adsorbent. International Journal of Biological Macromolecules **114**, 1279–1287 (2018).

62. Maurya, S. S., Nadar, S. S. & Rathod, V. K. Dual activity of laccase-lysine hybrid organic–inorganic nanoflowers for dye decolourization. Environmental Technology & Innovation **19**, 100798 (2020).
63. Patel, S. K. S. *et al.* Synthesis of cross-linked protein-metal hybrid nanoflowers and its application in repeated batch decolorization of synthetic dyes. Journal of Hazardous Materials **347**, 442–450 (2018).
64. Liu, Y. *et al.* Antigen-inorganic hybrid flowers-based vaccines with enhanced room temperature stability and effective anticancer immunity. Advanced Healthcare Materials **8**, 1900660 (2019).
65. Chauhan, P. S., Kumarasamy, M., Sosnik, A. & Danino, D. Enhanced thermostability and anticancer activity in breast cancer cells of laccase immobilized on pluronic-stabilized nanoparticles. ACS Applied Materials & Interfaces **11**, 39436–39448 (2019).
66. Chan, J. C. *et al.* Structural studies of *Myceliophthora thermophila* laccase in the presence of deep eutectic solvents. Enzyme and Microbial Technology **150**, 109890 (2021).
67. Khan, M., Husain, Q. & Bushra, R. Immobilization of β-galactosidase on surface modified cobalt/multiwalled carbon nanotube nanocomposite improves enzyme stability and resistance to inhibitor. International Journal of Biological Macromolecules **105**, 693–701 (2017).
68. Li, Y. X. *et al.* Highly effective removal of antibiotics from aqueous solution by magnetic $ZnFe_2O_4$/activated carbon composite. Water Science and Technology **82**, 877–886 (2020).
69. Wu, G. *et al.* Magnetic copper-based metal organic framework as an effective and recyclable adsorbent for removal of two fluoroquinolone antibiotics from aqueous solutions. Journal of Colloid and Interface Science **528**, 360–371 (2018).
70. Chen, Y. *et al.* Adsorptive removal and adsorption kinetics of fluoroquinolone by nano-hydroxyapatite. PLOS ONE **10**, e0145025 (2015).
71. Yilmaz, E., Ocsoy, I., Ozdemir, N. & Soylak, M. Bovine serum albumin-Cu(II) hybrid nanoflowers: An effective adsorbent for solid phase extraction and slurry sampling flame atomic absorption spectrometric analysis of cadmium and lead in water, hair, food and cigarette samples. Analytica Chimica Acta **906**, 110–117 (2016).
72. Parra Guardado, A. L., Belleville, M.-P., de Jesús Rostro Alanis, M., Parra Saldivar, R. & Sanchez-Marcano, J. Effect of redox mediators in pharmaceuticals degradation by laccase: A comparative study. Process Biochemistry **78**, 123–131 (2019).
73. Chen, Q. *et al.* Construction of immobilized 0D/1D heterostructure photocatalyst Au/CuS/CdS/TiO_2 NBs with enhanced photocatalytic activity towards moxifloxacin degradation. Chemical Engineering Journal **389**, 124476 (2020).
74. Rueda-Marquez, J. J., Levchuk, I., Fernández Ibañez, P. & Sillanpää, M. A critical review on application of photocatalysis for toxicity reduction of real wastewaters. Journal of Cleaner Production **258**, 120694 (2020).
75. Becker, D. *et al.* Removal of antibiotics in wastewater by enzymatic treatment with fungal laccase – Degradation of compounds does not always eliminate toxicity. Bioresource Technology **219**, 500–509 (2016).

76. Sturini, M. *et al.* Photolytic and photocatalytic degradation of fluoroquinolones in untreated river water under natural sunlight. Applied Catalysis B: Environmental **119–120**, 32–39 (2012).
77. Sturini, M. *et al.* Photodegradation of fluoroquinolones in surface water and antimicrobial activity of the photoproducts. Water Research **46**, 5575–5582 (2012).

Figures

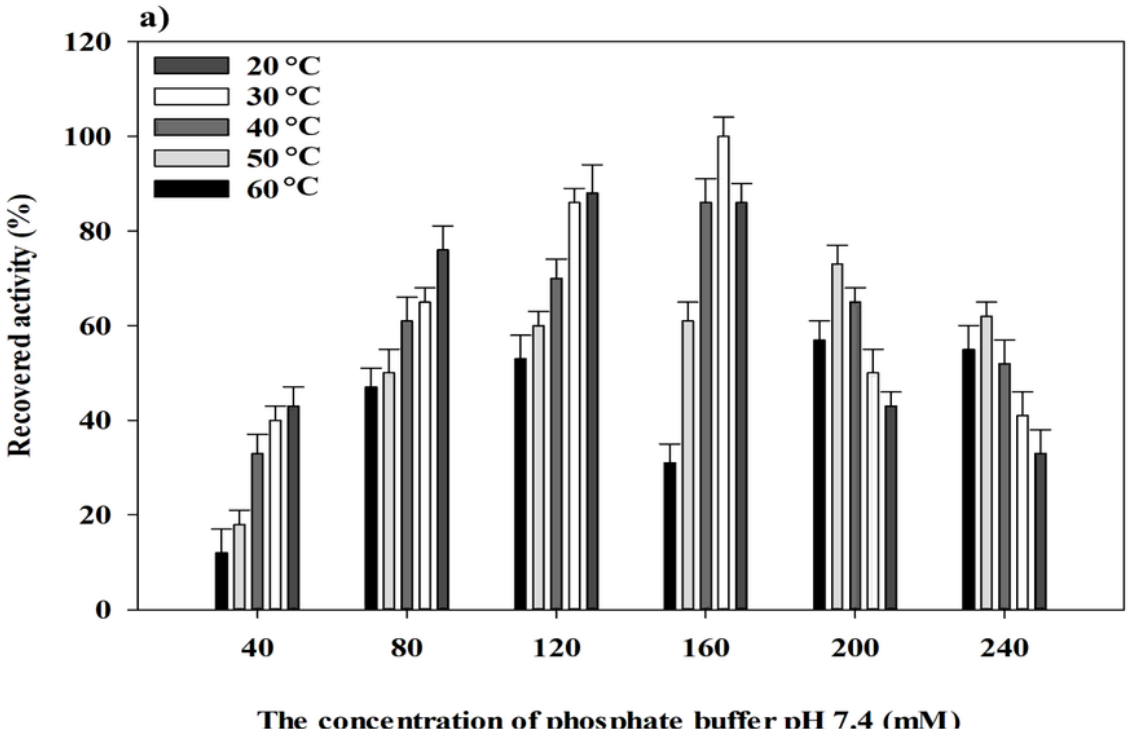

Figure 1

Optimization of the synthesis procedure. The synthesis of laccase@$Co_3(PO_4)_2$•HNFs by optimizing the concentration of phosphate and cobalt (II) ions (a), the influence of incubation (at 25 °C) as traditional procedures for the construction of HNFs on the recovered activity of the heterogeneous biocatalyst (b).

Figure 2

Scanning electron microscopy (SEM) imaging. SEM image (a, b), elemental map (c), and Energy dispersive X-Ray spectroscopy (EDX) analysis (d) of the constructed laccase@$Co_3(PO_4)_2$•HNFs.

Figure 3

X-ray diffraction (XRD) analysis. X-ray spectrum of laccase@$Co_3(PO_4)_2$•HNFs (a), XRD pattern of laccase@$Co_3(PO_4)_2$•HNFs and the standard $Co_3(PO_4)_2$ (JCPDS–00–027–1120) (b).

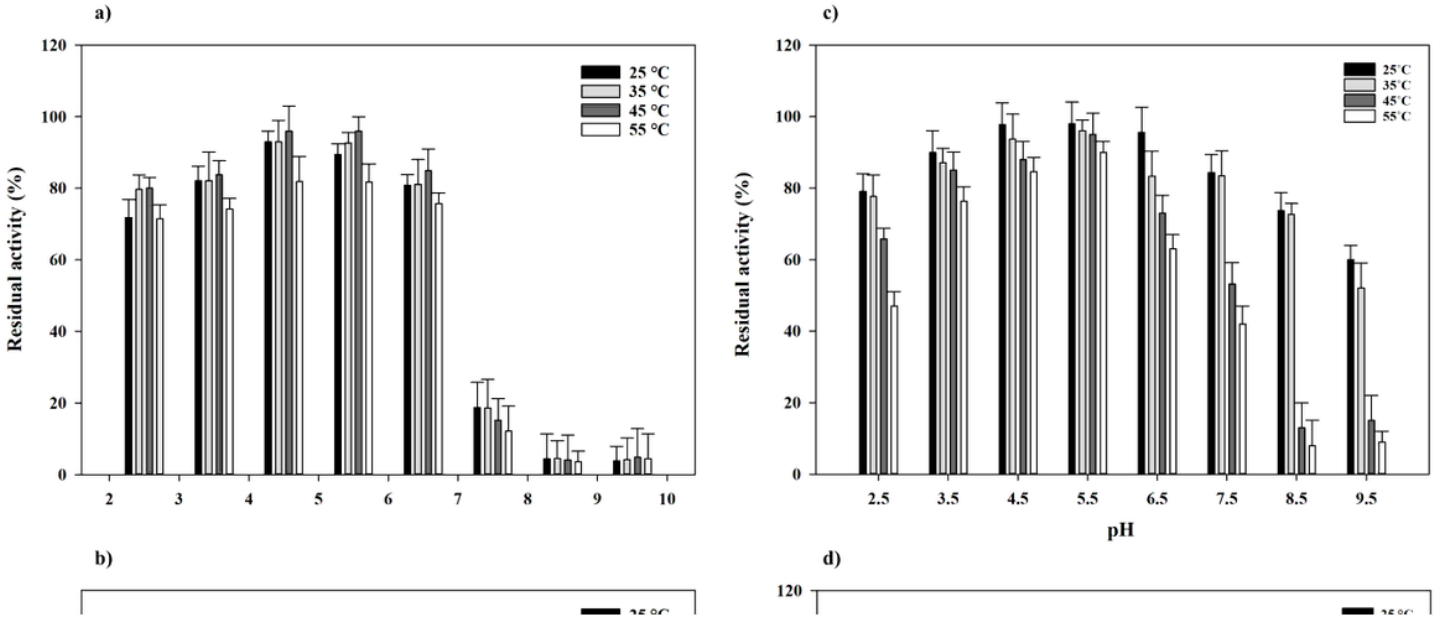

Figure 4

FT-IR analysis. The spectra of Fourier transform infrared (FTIR) spectroscopy of laccase@$Co_3(PO_4)_2$•HNFs (solid line), $Co_3(PO_4)_2$ (long dash line), and the free enzyme (dash-dot) (a). Reusability of laccase@$Co_3(PO_4)_2$•HNFs (b). The activity of laccase@$Co_3(PO_4)_2$•HNFs declined to under 50% of initial activity after 11 reusability cycles. Storage stability of laccase@$Co_3(PO_4)_2$•HNFs and the free laccase after 40 days of storage at 4 °C (c). Bioremoval of moxifloxacin by laccase@$Co_3(PO_4)_2$•HNFs and inactivated laccase@$Co_3(PO_4)_2$•HNFs. The experiments were conducted at 40 °C in phosphate buffer (10 mM, pH 4.5) (d).

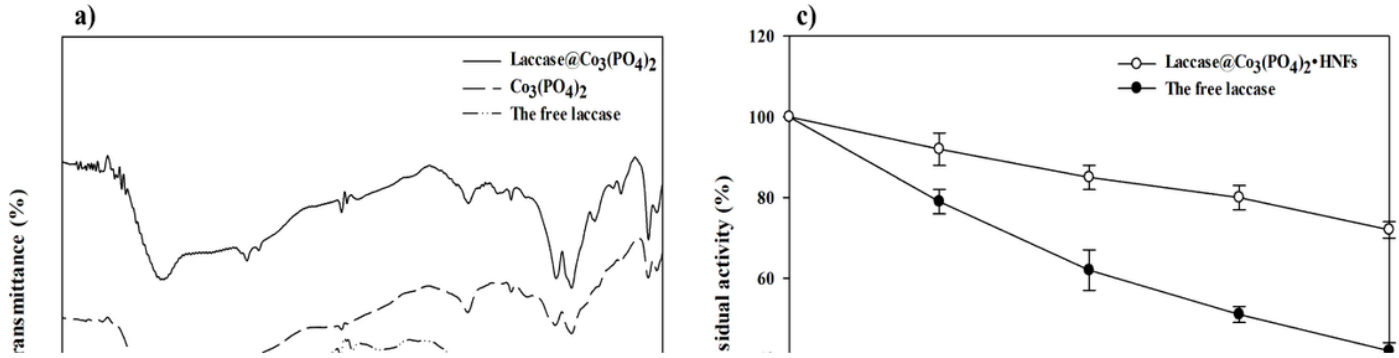

Figure 5

Stability and activity studies. Effect of pH and temperature on the activity (a) and stability of the free enzyme (c). Influence of pH and temperature on the activity (b) and stability of laccase@$Co_3(PO_4)_2$•HNFs (d).

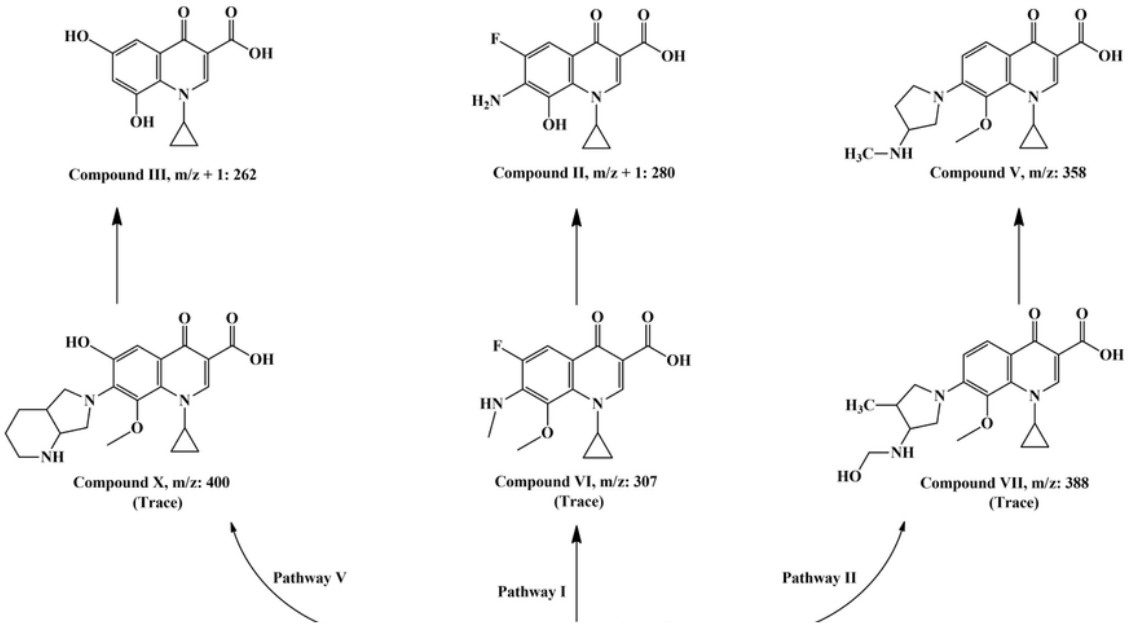

Figure 6

Mechanism of moxifloxacin degradation. Proposed moxifloxacin biotransformation pathways by laccase@$Co_3(PO_4)_2$•HNFs.

Supplementary Files

This is a list of supplementary files associated with this preprint. Click to download.

- SupplementaryMaterial.docx